

On the Convergence Rate of Projected Gradient Descent for a Back-Projection based Objective

Tom Tirer¹ Raja Giryes¹

Abstract

Ill-posed linear inverse problems appear in many fields of imaging science and engineering, and are typically addressed by solving optimization problems, which are composed of fidelity and prior terms or constraints. Traditionally, the research has been focused on different prior models, while the least squares (LS) objective has been the common choice for the fidelity term. However, recently a few works have considered a back-projection (BP) based fidelity term as an alternative to the LS, and demonstrated excellent reconstruction results for popular inverse problems. These prior works have also empirically shown that using the BP term, rather than the LS term, requires fewer iterations of plain and accelerated proximal gradient algorithms. In the current paper, we examine the convergence rate of the BP objective for the projected gradient descent (PGD) algorithm and identify an inherent source for its faster convergence compared to the LS objective. Numerical experiments with both ℓ_1 -norm and GAN-based priors corroborate our theoretical results for PGD. We also draw the connection to the observed behavior for proximal methods.

1. Introduction

The task of recovering a signal from its observations that are obtained by some acquisition process is common in many fields of science and engineering, and referred to as an *inverse problem*. In the field of image processing, the inverse problems are often linear, in the sense that the observations can be formulated by a linear model

$$\mathbf{y} = \mathbf{A}\mathbf{x} + \mathbf{e}, \quad (1)$$

where $\mathbf{x} \in \mathbb{R}^n$ represents the unknown original image, $\mathbf{y} \in \mathbb{R}^m$ represents the observations, \mathbf{A} is an $m \times n$ measurement

¹School of Electrical Engineering, Tel Aviv University, Tel Aviv, Israel. Correspondence to: Tom Tirer <tirer.tom@gmail.com>.

matrix and $\mathbf{e} \in \mathbb{R}^m$ is a noise vector. For example, this model corresponds to tasks like denoising (Rudin et al., 1992), deblurring (Danielyan et al., 2012), super-resolution (Yang et al., 2010), and compressed sensing (Donoho, 2006; Candès & Wakin, 2008).

A common strategy for recovering \mathbf{x} is to solve an optimization problem, which is composed of a fidelity term $\ell(\tilde{\mathbf{x}})$ that enforces agreement with the observations \mathbf{y} , and a prior term $s(\tilde{\mathbf{x}})$ ($\tilde{\mathbf{x}}$ is the optimization variable). Note that using a prior model is inevitable since the inverse problems represented by (1) are typically ill-posed. The optimization problem is usually stated in a penalized form

$$\min_{\tilde{\mathbf{x}}} \ell(\tilde{\mathbf{x}}) + \beta s(\tilde{\mathbf{x}}), \quad (2)$$

or in a constrained form

$$\min_{\tilde{\mathbf{x}}} \ell(\tilde{\mathbf{x}}) \quad \text{s.t.} \quad s(\tilde{\mathbf{x}}) \leq R, \quad (3)$$

where β and R are positive scalars that control the level of regularization. While a vast amount of research has focused on designing good prior models, most of the works use a typical least squares (LS) fidelity term

$$\ell_{LS}(\tilde{\mathbf{x}}) \triangleq \frac{1}{2} \|\mathbf{y} - \mathbf{A}\tilde{\mathbf{x}}\|_2^2, \quad (4)$$

where $\|\cdot\|_2$ stands for the Euclidean norm.

Recently, a new framework (Tirer & Giryes, 2018) has implicitly considered a different fidelity term, and has demonstrated excellent reconstruction results for popular tasks such as image deblurring (Tirer & Giryes, 2018) and super-resolution (Tirer & Giryes, 2019). Assuming that $m < n$ and $\text{rank}(\mathbf{A}) = m$ (which is the common case, e.g., in super-resolution and compressed sensing tasks), this fidelity term, which has been coined as “back-projection” (BP) term in (Tirer & Giryes, 2020), can be explicitly written as

$$\ell_{BP}(\tilde{\mathbf{x}}) \triangleq \frac{1}{2} \|\mathbf{A}^\dagger \mathbf{y} - \mathbf{A}^\dagger \mathbf{A} \tilde{\mathbf{x}}\|_2^2, \quad (5)$$

where $\mathbf{A}^\dagger \triangleq \mathbf{A}^T(\mathbf{A}\mathbf{A}^T)^{-1}$ is the pseudoinverse of \mathbf{A} , or in

an equivalent¹ weighted least-squares fashion

$$\ell_{BP}(\tilde{\mathbf{x}}) = \frac{1}{2} \|(\mathbf{A}\mathbf{A}^T)^{-\frac{1}{2}}(\mathbf{y} - \mathbf{A}\tilde{\mathbf{x}})\|_2^2. \quad (6)$$

The work in (Tirer & Giryes, 2020) has focused on examining and comparing the LS and BP terms from an estimation accuracy (MSE) point of view, and identified cases with advantages of the BP term over the LS term. Yet, the empirical results there also show that using the BP term, rather than the LS term, requires fewer iterations of plain and accelerated proximal gradient algorithms (e.g., ISTA and FISTA (Beck & Teboulle, 2009)) applied on the penalized formulation (2). This advantage implies reduced overall run-time if the operator \mathbf{A}^\dagger has fast implementation (e.g., in image deblurring and super-resolution) or if the proximal operation dominates the computational cost of each iteration. We emphasize that this behavior has not been mathematically analyzed in (Tirer & Giryes, 2020).

Contribution. In this paper, we provide mathematical reasoning for the faster convergence of BP compared to LS, for both projected gradient descent (PGD) applied on the constrained form (3), and the more general proximal gradient method applied on the penalized form (2). Our analysis for PGD (Section 3), which is inspired by the analysis in (Oymak et al., 2017), requires very mild assumptions and allows us to identify sources for the different convergence rates. Our analysis for proximal methods (Section 4, and Appendix B) requires a relaxed contraction condition on the proximal mapping of the prior, and further highlights the advantage of BP when $\mathbf{A}\mathbf{A}^T$ is badly conditioned. Numerical experiments (Section 5, and Appendix C) corroborate our theoretical results for PGD with both convex (ℓ_1 -norm) and non-convex (pre-trained DCGAN (Radford et al., 2015)) priors. For the ℓ_1 -norm prior, we also present experiments for proximal methods, and connect them with our analysis.

2. Preliminaries

Let us present notations and definitions that are used in the paper. We write $\|\cdot\|_2$ for the Euclidean norm of a vector, $\|\cdot\|$ for the spectral norm of a matrix, and $\sigma_{\max}(\cdot)$ and $\sigma_{\min}(\cdot)$ for the largest and smallest eigenvalue of a matrix, respectively. We denote the unit Euclidean ball and sphere in \mathbb{R}^n by \mathbb{B}^n and \mathbb{S}^{n-1} , respectively. We denote by $\mathcal{P}_{\mathcal{K}}(\cdot)$ the orthogonal projection onto a set \mathcal{K} . We denote by \mathbf{I}_n the identity matrix in \mathbb{R}^n , and by $\mathbf{P}_A \triangleq \mathbf{A}^\dagger \mathbf{A}$ and $\mathbf{Q}_A \triangleq \mathbf{I}_n - \mathbf{P}_A$ the orthogonal projections onto the row space and the null space (respectively) of the full row-rank matrix \mathbf{A} . Let us also define the descent set and its tangent cone as follows.

Definition 2.1. The descent set of the function $s(\cdot)$ at a

point \mathbf{x}_* is defined as

$$\mathcal{D}_s(\mathbf{x}_*) \triangleq \{\mathbf{h} \in \mathbb{R}^n : s(\mathbf{x}_* + \mathbf{h}) \leq s(\mathbf{x}_*)\}. \quad (7)$$

The tangent cone $\mathcal{C}_s(\mathbf{x}_*)$ at a point \mathbf{x}_* is the smallest closed cone satisfying $\mathcal{D}_s(\mathbf{x}_*) \subseteq \mathcal{C}_s(\mathbf{x}_*)$.

In this paper, we focus on minimizing (3) using PGD, i.e., by applying iterations of the form

$$\tilde{\mathbf{x}}_{t+1} = \mathcal{P}_{\mathcal{K}}(\tilde{\mathbf{x}}_t - \mu \nabla \ell(\tilde{\mathbf{x}}_t)), \quad (8)$$

where $\nabla \ell(\tilde{\mathbf{x}})$ is the gradient of $\ell(\cdot)$ at $\tilde{\mathbf{x}}$, μ is a step-size, and

$$\mathcal{K} \triangleq \{\tilde{\mathbf{x}} \in \mathbb{R}^n : s(\tilde{\mathbf{x}}) \leq R\}. \quad (9)$$

Note that

$$\begin{aligned} \nabla \ell_{LS}(\tilde{\mathbf{x}}) &= -\mathbf{A}^T(\mathbf{y} - \mathbf{A}\tilde{\mathbf{x}}), \\ \nabla \ell_{BP}(\tilde{\mathbf{x}}) &= -\mathbf{A}^\dagger(\mathbf{y} - \mathbf{A}\tilde{\mathbf{x}}). \end{aligned} \quad (10)$$

Therefore, we can examine a unified formulation of PGD for both objectives

$$\tilde{\mathbf{x}}_{t+1} = \mathcal{P}_{\mathcal{K}}(\tilde{\mathbf{x}}_t + \mu \mathbf{W}(\mathbf{y} - \mathbf{A}\tilde{\mathbf{x}}_t)), \quad (11)$$

where \mathbf{W} equals \mathbf{A}^T or \mathbf{A}^\dagger for the LS and BP terms, respectively.

3. Comparing PGD Convergence Rates

The goal of this section is to provide a mathematical reasoning for the observation (shown in Section 5) that using the BP term, rather than the LS term, requires fewer PGD iterations. We start in Section 3.1 with a warm-up example with a very restrictive prior that fixes the value of $\tilde{\mathbf{x}}$ on the null space of \mathbf{A} , which provides us with some intuition as to the advantage of BP. Then, in Sections 3.2 - 3.4 we build on the analysis technique in (Oymak et al., 2017) to show that the advantage of BP carries on to practical priors.

3.1. Warm-Up: Restrictive “Oracle” Prior

Let us define the following “oracle”² prior that fixes the value of $\tilde{\mathbf{x}}$ on the null space of \mathbf{A} to that of the latent \mathbf{x}

$$s_{\text{oracle}}(\tilde{\mathbf{x}}) = \begin{cases} 0, & \tilde{\mathbf{x}} : \mathbf{Q}_A \tilde{\mathbf{x}} = \mathbf{Q}_A \mathbf{x} \\ +\infty, & \text{otherwise} \end{cases}. \quad (12)$$

Applying the PGD update rule from (11) using this prior, we have

$$\tilde{\mathbf{x}}_{t+1} = \mathbf{P}_A(\tilde{\mathbf{x}}_t + \mu \mathbf{W}(\mathbf{y} - \mathbf{A}\tilde{\mathbf{x}}_t)) + \mathbf{Q}_A \mathbf{x}. \quad (13)$$

¹The equivalence can be seen by expanding the two quadratic forms.

²In fact, the results in this warm-up require that the prior fixes $\mathbf{Q}_A \tilde{\mathbf{x}}$ to a constant value on the null space of \mathbf{A} , but the value itself does not affect the convergence rates.

In the following, we specialize (13) for LS and BP with step-size of 1 over the Lipschitz constant of $\nabla\ell(\cdot)$. This step-size is perhaps the most common choice of practitioners, as it ensures (sublinear) convergence of the sequence $\{\tilde{x}_t\}$ for general convex priors (Beck & Teboulle, 2009) (i.e., for larger *constant* step-size PGD and general proximal methods may “swing” and not converge). Here, due to the constant Hessian matrix $\nabla^2\ell$ for LS and BP, this step-size can be computed as $\|\nabla^2\ell\|^{-1}$.

LS case. For the LS objective, we have $\mathbf{W} = \mathbf{A}^T$ and $\mu_{LS} = \|\nabla^2\ell_{LS}\|^{-1} = \|\mathbf{A}^T\mathbf{A}\|^{-1} = 1/\sigma_{\max}(\mathbf{A}\mathbf{A}^T)$. Therefore,

$$\begin{aligned}\tilde{x}_{t+1}^{LS} &= \mathbf{P}_A (\tilde{x}_t^{LS} + \mu_{LS}\mathbf{A}^T(\mathbf{y} - \mathbf{A}\tilde{x}_t^{LS})) + \mathbf{Q}_A\mathbf{x} \\ &= \mathbf{P}_A ((\mathbf{I}_n - \mu_{LS}\mathbf{A}^T\mathbf{A})\tilde{x}_t^{LS} + \mu_{LS}\mathbf{A}^T\mathbf{y}) + \mathbf{Q}_A\mathbf{x} \\ &= (\mathbf{P}_A - \mu_{LS}\mathbf{A}^T\mathbf{A})\tilde{x}_t^{LS} + \mu_{LS}\mathbf{A}^T\mathbf{y} + \mathbf{Q}_A\mathbf{x}.\end{aligned}\quad (14)$$

Let \mathbf{x}_*^{LS} be the stationary point of the sequence $\{\tilde{x}_t^{LS}\}$, i.e., $\mathbf{x}_*^{LS} = (\mathbf{P}_A - \mu_{LS}\mathbf{A}^T\mathbf{A})\mathbf{x}_*^{LS} + \mu_{LS}\mathbf{A}^T\mathbf{y} + \mathbf{Q}_A\mathbf{x}$. The convergence rate can be obtained as follows

$$\begin{aligned}\|\tilde{x}_{t+1}^{LS} - \mathbf{x}_*^{LS}\|_2 &= \|(\mathbf{P}_A - \mu_{LS}\mathbf{A}^T\mathbf{A})(\tilde{x}_t^{LS} - \mathbf{x}_*^{LS})\|_2 \\ &\leq \left(1 - \frac{\sigma_{\min}(\mathbf{A}\mathbf{A}^T)}{\sigma_{\max}(\mathbf{A}\mathbf{A}^T)}\right) \|\tilde{x}_t^{LS} - \mathbf{x}_*^{LS}\|_2.\end{aligned}\quad (15)$$

BP case. For the BP objective, we have $\mathbf{W} = \mathbf{A}^\dagger$ and $\mu_{BP} = \|\nabla^2\ell_{BP}\|^{-1} = \|\mathbf{A}^\dagger\mathbf{A}\|^{-1} = 1$, where the last equality follows from the fact that $\mathbf{P}_A = \mathbf{A}^\dagger\mathbf{A}$ is a non-trivial orthogonal projection. Substituting these terms in (13), we get

$$\begin{aligned}\tilde{x}_{t+1}^{BP} &= \mathbf{P}_A (\tilde{x}_t^{BP} + \mathbf{A}^\dagger(\mathbf{y} - \mathbf{A}\tilde{x}_t^{BP})) + \mathbf{Q}_A\mathbf{x} \\ &= \mathbf{P}_A (\mathbf{Q}_A\tilde{x}_t^{BP} + \mathbf{A}^\dagger\mathbf{y}) + \mathbf{Q}_A\mathbf{x} \\ &= \mathbf{A}^\dagger\mathbf{y} + \mathbf{Q}_A\mathbf{x}.\end{aligned}\quad (16)$$

Note that while the use of LS objective leads to linear convergence rate of $1 - \frac{\sigma_{\min}(\mathbf{A}\mathbf{A}^T)}{\sigma_{\max}(\mathbf{A}\mathbf{A}^T)}$, using BP objective requires only a *single* iteration. This result hints that an advantage of BP may exist even for practical priors $s(\tilde{x})$, which only implicitly impose some restrictions on $\mathbf{Q}_A\tilde{x}$.

3.2. General Analysis

The following theorem provides a term that characterizes the convergence rate of PGD for both LS and BP objectives for general priors. It is closely related to Theorem 2 in (Oymak et al., 2017). The difference is twofold. First, the theorem in (Oymak et al., 2017) considers only the LS objective and its derivation is not valid for the BP objective. Second, (Oymak et al., 2017) considers the estimation error, rather than only the convergence rate. Therefore, it examines

$\|\tilde{x}_t - \mathbf{x}\|_2$, where \mathbf{x} is the unknown “ground truth” signal, and assumes that $s(\mathbf{x})$ is known, which allows to set $R = s(\mathbf{x})$. In contrast, we generalize the theory for both LS and BP objectives, and for an arbitrary value of R . Among others, our theorem covers any stationary point \mathbf{x}_* of the PGD scheme (11) (i.e., an optimal point for convex s) for which $s(\mathbf{x}_*) = R$.³ The proof of the theorem is deferred to Appendix A.

Theorem 3.1. *Let $s : \mathbb{R}^n \rightarrow \mathbb{R}$ be a lower semi-continuous function,⁴ and let \mathbf{x}_* be a point on the boundary of \mathcal{K} , i.e., $s(\mathbf{x}_*) = R$. Let κ_s be a constant that is equal to 1 for convex s and equal to 2 otherwise. Then, the sequence $\{\tilde{x}_t\}$ obtained by (11) obeys*

$$\|\tilde{x}_{t+1} - \mathbf{x}_*\|_2 \leq \kappa_s \rho(\mathcal{C}_s(\mathbf{x}_*)) \|\tilde{x}_t - \mathbf{x}_*\|_2 + \kappa_s \mu \xi(\mathcal{C}_s(\mathbf{x}_*)), \quad (17)$$

where

$$\begin{aligned}\rho(\mathcal{C}_s(\mathbf{x}_*)) &\triangleq \sup_{\mathbf{u}, \mathbf{v} \in \mathcal{C}_s(\mathbf{x}_*) \cap \mathbb{B}^n} \mathbf{u}^T (\mathbf{I}_n - \mu \mathbf{W} \mathbf{A}) \mathbf{v}, \\ \xi(\mathcal{C}_s(\mathbf{x}_*)) &\triangleq \sup_{\mathbf{v} \in \mathcal{C}_s(\mathbf{x}_*) \cap \mathbb{B}^n} \mathbf{v}^T \mathbf{W} (\mathbf{y} - \mathbf{A} \mathbf{x}_*).\end{aligned}\quad (18)$$

Theorem 3.1 is meaningful, i.e., implies convergence and provides characterization of its rate, if $\kappa_s \rho(\mathcal{C}_s(\mathbf{x}_*)) < 1$. We elaborate on this issue for LS and BP, below Propositions 3.2 and 3.3, respectively.

Assuming that $\kappa_s \rho(\mathcal{C}_s(\mathbf{x}_*)) < 1$, the term $\xi(\mathcal{C}_s(\mathbf{x}_*))$ belongs to the component of the bound (17) which cannot be compensated for by using more iterations. Note that if $R = s(\mathbf{x})$, then Theorem 3.1 can be applied with $\mathbf{x}_* = \mathbf{x}$. In this case, $\xi(\mathcal{C}_s(\mathbf{x}_*)) = \xi(\mathcal{C}_s(\mathbf{x}))$ characterizes the estimation error $\lim_{t \rightarrow \infty} \|\tilde{x}_t - \mathbf{x}\|_2$ (up to a factor due to the recursion in (17)). Moreover, $\mathbf{y} - \mathbf{A}\mathbf{x}_* = \mathbf{y} - \mathbf{A}\mathbf{x} = \mathbf{e}$, so the term $\xi(\mathcal{C}_s(\mathbf{x}))$ vanishes if there is no noise.

In practice, one does not know the value of $s(\mathbf{x})$ and often R that is not equal to $s(\mathbf{x})$ provides better results in the presence of noise or when $s(\cdot)$ is non-convex. Therefore, in this work we choose to compare the convergence rates for LS and BP objectives for arbitrary values of R . As we consider arbitrary R , we focus on $\mathbf{x}_* = \lim_{t \rightarrow \infty} \tilde{x}_t$, i.e., the stationary point obtained by PGD. In this case $\lim_{t \rightarrow \infty} \|\tilde{x}_t - \mathbf{x}_*\|_2 = 0$, and thus the component with $\xi(\mathcal{C}_s(\mathbf{x}_*))$ in (17) presents slackness that is a consequence of the proof technique. To further see that $\xi(\mathcal{C}_s(\mathbf{x}_*))$ is not expected to affect the conclusions of our analysis, note that we examine PGD with step-sizes that ensure convergence in convex settings (Beck & Teboulle, 2009) (namely, with the common step-size of $\|\nabla^2\ell\|^{-1}$). Therefore, for convex

³Essentially, we require that R is small enough such that the prior is not meaningless.

⁴A lower semi-continuous function is a function whose sub-level sets are closed.

$s(\cdot)$ misbehavior of $\{\tilde{\mathbf{x}}_t\}$ like “swinging” is not possible. Empirically, monotonic convergence of $\{\tilde{\mathbf{x}}_t\}$ is observed in Section 5 even for highly non-convex prior such as DCGAN.

In the rest of this section we focus on the term $\rho(\mathcal{C}_s(\mathbf{x}_*))$ in (17). Whenever $\kappa_s \rho(\mathcal{C}_s(\mathbf{x}_*)) < 1$, this term characterizes the convergence rate of PGD: *smaller ρ implies faster convergence*. We start with specializing and bounding it for $\ell_{LS}(\tilde{\mathbf{x}})$ and $\ell_{BP}(\tilde{\mathbf{x}})$.

Proposition 3.2. *Consider the LS objective $\ell_{LS}(\tilde{\mathbf{x}})$ and step-size $\mu_{LS} \triangleq \|\nabla^2 \ell_{LS}\|^{-1}$. We have*

$$\rho(\mathcal{C}_s(\mathbf{x}_*)) \leq P_{LS}(\mathcal{C}_s(\mathbf{x}_*)), \quad (19)$$

where

$$P_{LS}(\mathcal{C}_s(\mathbf{x}_*)) \triangleq 1 - \frac{1}{\|\mathbf{A}^T \mathbf{A}\|} \inf_{\mathbf{u} \in \mathcal{C}_s(\mathbf{x}_*) \cap \mathbb{S}^{n-1}} \|\mathbf{A} \mathbf{u}\|_2^2. \quad (20)$$

Proof. For the LS objective, we have $\mathbf{W} = \mathbf{A}^T$ and $\mu_{LS} = \|\nabla^2 \ell_{LS}\|^{-1} = \|\mathbf{A}^T \mathbf{A}\|^{-1}$. Therefore, $\mathbf{I}_n - \mu_{LS} \mathbf{A}^T \mathbf{A}$ is positive semi-definite, and using the generalized Cauchy-Schwarz inequality we get

$$\begin{aligned} \rho(\mathcal{C}_s(\mathbf{x}_*)) &= \sup_{\mathbf{u}, \mathbf{v} \in \mathcal{C}_s(\mathbf{x}_*) \cap \mathbb{S}^{n-1}} \mathbf{u}^T (\mathbf{I}_n - \mu_{LS} \mathbf{A}^T \mathbf{A}) \mathbf{v} \\ &\leq \sup_{\mathbf{u}, \mathbf{v} \in \mathcal{C}_s(\mathbf{x}_*) \cap \mathbb{S}^{n-1}} \sqrt{\mathbf{u}^T (\mathbf{I}_n - \mu_{LS} \mathbf{A}^T \mathbf{A}) \mathbf{u}} \\ &\quad \cdot \sqrt{\mathbf{v}^T (\mathbf{I}_n - \mu_{LS} \mathbf{A}^T \mathbf{A}) \mathbf{v}} \\ &= \sup_{\mathbf{u} \in \mathcal{C}_s(\mathbf{x}_*) \cap \mathbb{S}^{n-1}} \mathbf{u}^T (\mathbf{I}_n - \mu_{LS} \mathbf{A}^T \mathbf{A}) \mathbf{u} \\ &= 1 - \mu_{LS} \inf_{\mathbf{u} \in \mathcal{C}_s(\mathbf{x}_*) \cap \mathbb{S}^{n-1}} \|\mathbf{A} \mathbf{u}\|_2^2 = P_{LS}(\mathcal{C}_s(\mathbf{x}_*)). \end{aligned} \quad (21)$$

□

Various works (Chandrasekaran et al., 2012; Plan & Vershynin, 2012; Amelunxen et al., 2014; Genzel et al., 2017) have proved, via Gordon’s lemma (Corollary 1.2 in (Gordon, 1988)) and the notion of *Gaussian width*, that if: 1) the entries of $\mathbf{A} \in \mathbb{R}^{m \times n}$ are i.i.d Gaussians $\mathcal{N}(0, \frac{1}{m})$; 2) \mathbf{x}_* belongs to a parsimonious signal model (e.g., a sparse signal); and 3) $s(\cdot)$ is an appropriate prior for the signal model (e.g., ℓ_0 -quasi-norm or ℓ_1 -norm for sparse signals), then there exist tight lower bounds⁵ on the restricted smallest eigenvalue of \mathbf{A} : $\inf_{\mathbf{u} \in \mathcal{C}_s(\mathbf{x}_*) \cap \mathbb{S}^{n-1}} \|\mathbf{A} \mathbf{u}\|_2^2$, which are much

greater than the naive lower bound $\sigma_{\min}(\mathbf{A}^T \mathbf{A}) \|\mathbf{u}\|_2^2 = 0$ (recall that $m < n$, so $\sigma_{\min}(\mathbf{A}^T \mathbf{A}) = 0$). Together with the (small enough) step-size μ_{LS} , this implies that $\kappa_s P_{LS}(\mathcal{C}_s(\mathbf{x}_*)) < 1$ and therefore Theorem 3.1 indeed provides meaningful guarantees for PGD applied on LS objective under the above conditions.

⁵The tightness of these bounds has been shown empirically.

Proposition 3.3. *Consider the BP objective $\ell_{BP}(\tilde{\mathbf{x}})$ and step-size $\mu_{BP} \triangleq \|\nabla^2 \ell_{BP}\|^{-1}$. We have*

$$\rho(\mathcal{C}_s(\mathbf{x}_*)) \leq P_{BP}(\mathcal{C}_s(\mathbf{x}_*)), \quad (22)$$

where

$$P_{BP}(\mathcal{C}_s(\mathbf{x}_*)) \triangleq 1 - \inf_{\mathbf{u} \in \mathcal{C}_s(\mathbf{x}_*) \cap \mathbb{S}^{n-1}} \|(\mathbf{A} \mathbf{A}^T)^{-\frac{1}{2}} \mathbf{A} \mathbf{u}\|_2^2. \quad (23)$$

Proof. For the BP objective, we have $\mathbf{W} = \mathbf{A}^\dagger = \mathbf{A}^T (\mathbf{A} \mathbf{A}^T)^{-1}$ and $\mu_{BP} = \|\nabla^2 \ell_{BP}\|^{-1} = \|\mathbf{A}^\dagger \mathbf{A}\|^{-1} = 1$. Since $\mathbf{I}_n - \mu_{BP} \mathbf{A}^\dagger \mathbf{A}$ is positive semi-definite, using similar steps as those in (21) we get

$$\begin{aligned} \rho(\mathcal{C}_s(\mathbf{x}_*)) &= \sup_{\mathbf{u}, \mathbf{v} \in \mathcal{C}_s(\mathbf{x}_*) \cap \mathbb{S}^{n-1}} \mathbf{u}^T (\mathbf{I}_n - \mu_{BP} \mathbf{A}^\dagger \mathbf{A}) \mathbf{v} \\ &\leq 1 - \mu_{BP} \inf_{\mathbf{u} \in \mathcal{C}_s(\mathbf{x}_*) \cap \mathbb{S}^{n-1}} \|(\mathbf{A} \mathbf{A}^T)^{-\frac{1}{2}} \mathbf{A} \mathbf{u}\|_2^2 \\ &= P_{BP}(\mathcal{C}_s(\mathbf{x}_*)). \end{aligned} \quad (24)$$

□

As shown in Proposition 3.4 below, if $P_{LS}(\mathcal{C}_s(\mathbf{x}_*)) < 1$ then $P_{BP}(\mathcal{C}_s(\mathbf{x}_*)) < 1$ as well. Therefore, Theorem 3.1 provides meaningful guarantees also for PGD applied on BP objective. However, obtaining tight lower bounds directly on the restricted smallest eigenvalue $\inf_{\mathbf{u} \in \mathcal{C}_s(\mathbf{x}_*) \cap \mathbb{S}^{n-1}} \|(\mathbf{A} \mathbf{A}^T)^{-\frac{1}{2}} \mathbf{A} \mathbf{u}\|_2^2$, similar to those obtained (in some cases) for $\inf_{\mathbf{u} \in \mathcal{C}_s(\mathbf{x}_*) \cap \mathbb{S}^{n-1}} \|\mathbf{A} \mathbf{u}\|_2^2$, appears to be an open problem. Its difficulty stems from the fact that tools like Slepian’s lemma and Sudakov-Fernique inequality, which are the core of Gordon’s lemma that is used to bound $\inf_{\mathbf{u} \in \mathcal{C}_s(\mathbf{x}_*) \cap \mathbb{S}^{n-1}} \|\mathbf{A} \mathbf{u}\|_2^2$, cannot be used in this case.

Denote by \mathbf{x}_*^{LS} and \mathbf{x}_*^{BP} the recoveries obtained by LS and BP objectives, respectively. The terms $P_{LS}(\mathcal{C}_s(\mathbf{x}_*^{LS}))$ and $P_{BP}(\mathcal{C}_s(\mathbf{x}_*^{BP}))$ upper bound the convergence rate ρ for each objective. Observing these expressions, we identify two factors that affect their relation, and are thus possible sources for different convergence rates. The two factors, labeled as “intrinsic” and “extrinsic”, are explained in Sections 3.3 and 3.4, respectively.

3.3. Intrinsic Source of Faster Convergence for BP

The following proposition addresses the case where the obtained minimizers are similar, i.e., $\mathbf{x}_*^{LS} \approx \mathbf{x}_*^{BP}$. It guarantees that $P_{BP}(\mathcal{C}_s(\mathbf{x}_*))$ is lower than $P_{LS}(\mathcal{C}_s(\mathbf{x}_*))$ for any full row-rank \mathbf{A} .

Proposition 3.4. *Consider $P_{LS}(\mathcal{C}_s(\mathbf{x}_*))$ and $P_{BP}(\mathcal{C}_s(\mathbf{x}_*))$ defined in (20) and (23). We have*

$$P_{BP}(\mathcal{C}_s(\mathbf{x}_*)) \leq P_{LS}(\mathcal{C}_s(\mathbf{x}_*)). \quad (25)$$

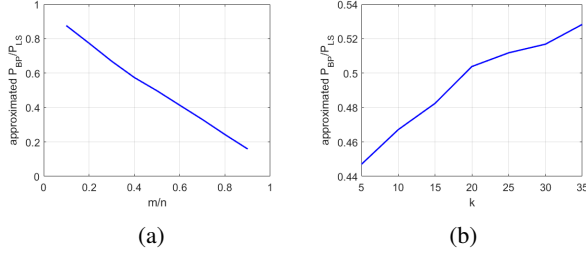


Figure 1: Approximate ratio P_{BP}/P_{LS} for k -sparse $\mathbf{u} \in \mathbb{R}^{1024}$ and Gaussian \mathbf{A} (see the text for details) for: (a) $k = 20$ and m is varied; (b) $m = 512$ and k is varied.

Proof.

$$\begin{aligned}
 P_{BP}(\mathcal{C}_s(\mathbf{x}_*)) &= 1 - \inf_{\mathbf{u} \in \mathcal{C}_s(\mathbf{x}_*) \cap \mathbb{S}^{n-1}} \|(\mathbf{A}\mathbf{A}^T)^{-\frac{1}{2}} \mathbf{A}\mathbf{u}\|_2^2 \\
 &\leq 1 - \sigma_{\min}((\mathbf{A}\mathbf{A}^T)^{-1}) \inf_{\mathbf{u} \in \mathcal{C}_s(\mathbf{x}_*) \cap \mathbb{S}^{n-1}} \|\mathbf{A}\mathbf{u}\|_2^2 \\
 &= 1 - \frac{1}{\|\mathbf{A}^T \mathbf{A}\|} \inf_{\mathbf{u} \in \mathcal{C}_s(\mathbf{x}_*) \cap \mathbb{S}^{n-1}} \|\mathbf{A}\mathbf{u}\|_2^2 = P_{LS}(\mathcal{C}_s(\mathbf{x}_*))
 \end{aligned} \tag{26}$$

□

Notice that in (26) we use an inequality that does not take into account the fact that \mathbf{u} resides in a restricted set. As discussed above, this is due to the lack of tighter lower bounds for $\inf_{\mathbf{u} \in \mathcal{C} \cap \mathbb{S}^{n-1}} \|(\mathbf{A}\mathbf{A}^T)^{-\frac{1}{2}} \mathbf{A}\mathbf{u}\|_2^2$. Still, following the warm-up example⁶ and the discussions below Propositions 3.2 and 3.3, we conjecture that the inequality in Proposition 3.4 is strict, i.e., that $P_{BP}(\mathcal{C}_s(\mathbf{x}_*)) < P_{LS}(\mathcal{C}_s(\mathbf{x}_*))$, in generic cases when the entries of $\mathbf{A} \in \mathbb{R}^{m \times n}$ are i.i.d Gaussians $\mathcal{N}(0, \frac{1}{m})$, the recovered signals belong to parsimonious models and feasible sets are appropriately chosen.

Let us present an experiment that supports our conjecture. We consider a Gaussian \mathbf{A} , as mentioned above, and \mathcal{C} which is the set of k -sparse signals, i.e., the number of non-zero elements in any $\mathbf{u} \in \mathcal{C}$ is at most k . In this case, $\inf_{\mathbf{u} \in \mathcal{C} \cap \mathbb{S}^{n-1}} \|\mathbf{A}\mathbf{u}\|_2^2$ can be approximated by: 1) drawing many supports, i.e., choices of k out of the n columns of \mathbf{A} ; 2) for each support creating an $m \times k$ matrix $\tilde{\mathbf{A}}$ and computing $\sigma_{\min}(\tilde{\mathbf{A}}^T \tilde{\mathbf{A}})$; and 3) keeping the minimal value. Plugging the approximation of $\inf_{\mathbf{u} \in \mathcal{C} \cap \mathbb{S}^{n-1}} \|\mathbf{A}\mathbf{u}\|_2^2$ in (20), we obtain an approximation of $P_{LS}(\mathcal{C})$.

Similarly, to approximate $\inf_{\mathbf{u} \in \mathcal{C} \cap \mathbb{S}^{n-1}} \|(\mathbf{A}\mathbf{A}^T)^{-\frac{1}{2}} \mathbf{A}\mathbf{u}\|_2^2$ the same procedure can be done with $\sigma_{\min}(\tilde{\mathbf{A}}^T (\mathbf{A}\mathbf{A}^T)^{-1} \tilde{\mathbf{A}})$.

⁶Note that the general analysis subsumes the warm-up result (strict inequality for the convergence rates). For the prior in (12) we have that the descent set (and its tangent cone) are the subspace spanned by the rows of \mathbf{A} . Therefore, we have that $P_{LS} = 1 - \frac{\sigma_{\min}(\mathbf{A}\mathbf{A}^T)}{\|\mathbf{A}^T \mathbf{A}\|}$ and $P_{BP} = 1 - \|\mathbf{P}_A\| = 0$.

Plugging the approximation of $\inf_{\mathbf{u} \in \mathcal{C} \cap \mathbb{S}^{n-1}} \|(\mathbf{A}\mathbf{A}^T)^{-\frac{1}{2}} \mathbf{A}\mathbf{u}\|_2^2$ in (23), we obtain an approximation of $P_{BP}(\mathcal{C})$.

Fig. 1a shows the approximate ratio $\hat{P}_{BP}/\hat{P}_{LS}$ for $n = 1024$, $k = 20$ and different values of m . Fig. 1b shows this ratio for $n = 1024$, $m = 512$ and different values of k . In both figures \hat{P}_{BP} is *strictly* smaller than \hat{P}_{LS} , which agrees with our conjecture.

Discussion. As we have obtained (worst-case) upper bounds on PGD convergence rates for LS and BP, a natural question is: Should the bounds be tight in order to deduce conclusions on the relation of the *real* rates for LS and BP? Interestingly, when both objectives lead to a similar stationary point \mathbf{x}_* , note that it is *enough* to verify that $P_{LS}(\mathcal{C}_s(\mathbf{x}_*))$ is tight to conclude that the real rate for BP is better than for LS. This follows from the fact that the real rate of BP is smaller (i.e., better) than $P_{BP}(\mathcal{C}_s(\mathbf{x}_*))$, and $P_{BP}(\mathcal{C}_s(\mathbf{x}_*)) \leq P_{LS}(\mathcal{C}_s(\mathbf{x}_*))$. That is, while tightness in P_{LS} is important (and is indeed obtained in certain cases, as discussed above and empirically demonstrated in (Oymak et al., 2017)), “miss-tightness” in P_{BP} only increases the gap between the *real* rates of LS and BP in favor of BP!

3.4. Extrinsic Source of Different Convergence Rates

Since using LS and BP objectives in (3) defines two different optimization problems, potentially, one may prefer to assign different values for the regularization parameter R in each case. This is obviously translated to using feasible sets with different volume. Note that the obtained convergence rates depend on the feasible set through $\mathcal{D}_s(\mathbf{x}_*)$ and $\mathcal{C}_s(\mathbf{x}_*)$, and are therefore affected by the value of R . We refer to this effect on the convergence rate as “extrinsic” because it originates in a modified prior rather than directly from the different BP and LS objectives.

For the LS objective, under the assumption of Gaussian \mathbf{A} , the work by (Oymak et al., 2017) has used the notion of Gaussian width to theoretically link the complexity of the signal prior, which translates to the feasible set in (3), and the convergence rate of PGD. Their result implies that *increasing* the size of the feasible set (due to a relaxed prior) is expected to *decrease* the convergence rate, i.e., slow down PGD. Therefore, it is expected that using $R_{BP} < R_{LS}$ would increase the gap between the convergence rates in favor of the BP term, beyond the effect of its intrinsic advantage described in Section 3.3. On the other hand, using $R_{BP} > R_{LS}$ may counteract the intrinsic advantage of the BP term.

4. Convergence Analysis Beyond PGD

Many works on inverse problems use the penalized optimization problem (2) rather than the constrained one (3).

Oftentimes (2) is minimized using the proximal gradient method, which is given by

$$\tilde{\mathbf{x}}_{t+1} = \text{prox}_{\mu\beta s(\cdot)}(\tilde{\mathbf{x}}_t - \mu\nabla\ell(\tilde{\mathbf{x}}_t)), \quad (27)$$

where

$$\text{prox}_{s(\cdot)}(\tilde{\mathbf{z}}) \triangleq \underset{\tilde{\mathbf{x}}}{\text{argmin}} \frac{1}{2}\|\tilde{\mathbf{z}} - \tilde{\mathbf{x}}\|_2^2 + s(\tilde{\mathbf{x}}) \quad (28)$$

is the proximal mapping $s(\cdot)$ at the point $\tilde{\mathbf{z}}$, which was introduced for convex functions in (Moreau, 1965). Note that PGD with convex feasible set is essentially the proximal gradient method for $s(\cdot)$ which is a convex indicator, and similarly to PGD, setting the step-size μ to 1 over the Lipschitz constant of $\nabla\ell(\cdot)$ ensures sublinear convergence of (27) in convex settings (Beck & Teboulle, 2009).

To obtain an expression that allows to compare the convergence rates of (27) with $\ell_{LS}(\tilde{\mathbf{x}})$ and $\ell_{BP}(\tilde{\mathbf{x}})$, we make a relaxed contraction assumption. Namely, we require that the proximal mapping of $\beta s(\cdot)$ is a contraction (only) in the null space of \mathbf{A} (rather than in all \mathbb{R}^n).

Condition B.2. *Given the convex function $\beta s(\cdot)$ and the full row-rank matrix \mathbf{A} , there exists $0 < \sigma_{\mathbf{A},\beta s(\cdot)} \leq 1$ such that for all $\tilde{\mathbf{z}}_1, \tilde{\mathbf{z}}_2$*

$$\|\text{prox}_{\beta s(\cdot)}(\tilde{\mathbf{z}}_1) - \text{prox}_{\beta s(\cdot)}(\tilde{\mathbf{z}}_2)\|_2 \leq \|(\mathbf{P}_A + (1 - \sigma_{\mathbf{A},\beta s(\cdot)})\mathbf{Q}_A)(\tilde{\mathbf{z}}_1 - \tilde{\mathbf{z}}_2)\|_2. \quad (29)$$

Note that the constant $\sigma_{\mathbf{A},\beta s(\cdot)}$ reflects the restriction that $\beta s(\cdot)$ imposes on the null space of \mathbf{A} . Condition B.2 is satisfied by priors such as Tikhonov regularization (Tikhonov, 1963) or even a recent GMM-based prior (Teodoro et al., 2018). See Appendix B for more details on this condition.

Under Condition B.2, we prove (Theorem B.3 in Appendix B) that the proximal gradient method with step-size of $\|\nabla^2\ell\|^{-1}$ exhibits *linear* convergence, with rate that shows an advantage of the BP term over the LS term, due to a better “restricted condition number” of the Hessian of ℓ_{BP} in the subspace spanned by the rows of \mathbf{A} . Informally, we have

$$\begin{aligned} \frac{\|\tilde{\mathbf{x}}_{t+1}^{LS} - \mathbf{x}_*^{LS}\|_2}{\|\tilde{\mathbf{x}}_t^{LS} - \mathbf{x}_*^{LS}\|_2} &\leq \max \left\{ 1 - \frac{\sigma_{\min}(\mathbf{A}\mathbf{A}^T)}{\sigma_{\max}(\mathbf{A}\mathbf{A}^T)}, 1 - \tilde{\sigma}_{LS} \right\}, \\ \frac{\|\tilde{\mathbf{x}}_{t+1}^{BP} - \mathbf{x}_*^{BP}\|_2}{\|\tilde{\mathbf{x}}_t^{BP} - \mathbf{x}_*^{BP}\|_2} &\leq 1 - \tilde{\sigma}_{BP}, \end{aligned} \quad (30)$$

where $\tilde{\sigma}_{LS} = \sigma_{\mathbf{A}, \frac{\beta_{LS}}{\sigma_{\max}(\mathbf{A}\mathbf{A}^T)} s(\cdot)}$ and $\tilde{\sigma}_{BP} = \sigma_{\mathbf{A}, \beta_{BP} s(\cdot)}$. Note that if $\tilde{\sigma}_{LS} < \tilde{\sigma}_{BP}$ then the bound on the rate of BP is better, regardless of $\frac{\sigma_{\min}(\mathbf{A}\mathbf{A}^T)}{\sigma_{\max}(\mathbf{A}\mathbf{A}^T)}$. Alternatively, this result hints that a worse condition number of $\mathbf{A}\mathbf{A}^T$ is expected to correlate with a larger difference between the convergence rates of LS and BP *in favor of BP*. Since PGD with

convex feasible set is a special case of proximal gradient method, this behavior is also expected for PGD. Indeed, this is demonstrated for compressed sensing in Appendix C.

In this paper we mainly focus on direct PGD results (rather than on those obtained for general proximal methods) for two reasons. Firstly, they do not require a contractive assumption. Secondly, identifying an “intrinsic factor” for different convergence rates is easier for PGD both in experiments (see the discussion on Fig. 3) and analysis (the dependence of $\tilde{\sigma}_{LS}, \tilde{\sigma}_{BP}$ on β_{LS}, β_{BP} is not explicit, and the effect of the regularization parameters on the results cannot be bypassed by assuming $\mathbf{x}_*^{LS} \approx \mathbf{x}_*^{BP}$, as we have done in Section 3.3 for R_{LS} and R_{BP} in PGD).

5. Experiments

In this section, we provide numerical experiments that corroborate our mathematical analysis for both convex (ℓ_1 -norm) and non-convex (pre-trained DCGAN (Radford et al., 2015)) priors. For the ℓ_1 -norm prior, we examine the performance of PGD with LS and BP objectives for compressed sensing (CS). It is demonstrated that both objectives prefer (i.e., provide better PSNR for) a similar value of R — a case in which the faster convergence for BP is dictated by its “intrinsic” advantage, rather than by an “extrinsic” source. For this prior, we also examine an accelerated proximal gradient method (FISTA (Beck & Teboulle, 2009)) applied on (2) with LS and BP fidelity terms, and suggest an explanation for the observed behavior using the “extrinsic” and “intrinsic” sources. For the DCGAN prior we examine the performance of PGD for CS and super-resolution (SR) tasks, and show again the inherent advantage of the BP objective.

5.1. ℓ_1 -Norm Prior

We consider a typical CS scenario⁷, where the measurement matrix is Gaussian (with i.i.d. entries drawn from $\mathcal{N}(0, 1/m)$), the compression ratio is $m/n = 0.5$, and the signal-to-noise ratio (SNR) is 20dB (with white Gaussian noise). We use four standard test images: *cameraman*, *house*, *peppers*, and *Lena*, in their 128×128 versions (so $n = 128^2$). To apply sparsity-based recovery, we represent the images in the Haar wavelet basis, i.e., \mathbf{A} is the multiplication of the $m \times n$ Gaussian measurement matrix with an $n \times n$ Haar wavelet basis.

For the reconstruction, we use the feasible set $\mathcal{K} = \{\tilde{\mathbf{x}} \in \mathbb{R}^n : \|\tilde{\mathbf{x}}\|_1 \leq R\}$, where $\|\cdot\|_1$ is the ℓ_1 -norm, and project on it using the fast algorithm from (Duchi et al., 2008). Starting from $\tilde{\mathbf{x}}_0 = 0$, we apply 1000 iterations of PGD on the BP and LS objectives with the typical step-size of 1 over the spectral norm of the objective’s Hessian. We compute \mathbf{A}^\dagger in advance, so the PGD iterations for both

⁷See Appendix C for more scenarios.

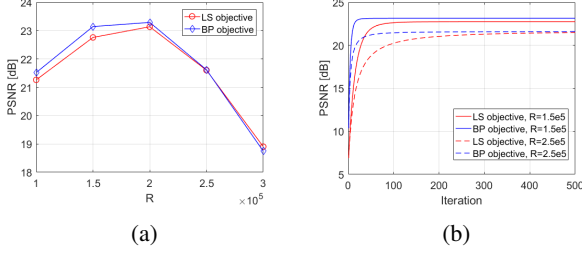


Figure 2: Compressed sensing with $m/n = 0.5$ Gaussian measurements and SNR of 20dB. PSNR (averaged over 4 test images) of PGD with ℓ_1 prior versus: (a) regularization parameter R (for 1000 iterations); (b) iteration number (for $R = 1.5e5$ and $R = 2.5e5$).

objectives have similar computational cost.

Fig. 2a shows the PSNR of the reconstructions, averaged over all images, for different values of the regularization parameter R . Fig. 2b shows the average PSNR as a function of the iteration number, for $R = 1.5e5$ and $R = 2.5e5$. Note that $R = 2.5e5$ yields less accurate results despite being the average ℓ_1 -norm of the four “ground truth” test images (in Haar basis representation). From Fig. 2b we see that when PGD is applied on BP and LS objectives with the same value of R , indeed BP is faster, which demonstrates its “intrinsic” advantage. Also, when R is increased, the convergence of PGD for both objectives becomes slower due to this “extrinsic” modification. Note, though, that Fig. 2a implies that both objectives prefer a similar value of R . Therefore, when R is (uniformly) tuned for best PSNR of each method, it is expected that the intrinsic advantage of BP over LS is the reason for its faster PGD convergence.

We turn to recover the images by minimization of (2) using 1000 iterations of FISTA (Beck & Teboulle, 2009) with LS and BP fidelity terms. Figs. 3a and 3b show the average PSNR vs. β and vs. iteration number, respectively. Fig. 4 presents the average $\|\mathbf{x}_*\|_1$ of the recoveries vs. β . Note that the best PSNRs for BP and LS are received by values of β for which $\|\mathbf{x}_*\|_1$ is very similar for both terms, i.e., the equivalent constrained LS and BP formulations have very similar R (as observed for PGD).

However, disentangling the factors for different convergence rates of LS and BP, where for each of them the regularization parameter is (uniformly) tuned for best PSNR, is more complicated for proximal methods than for PGD. To see this, note that in Figs. 3a and 4, for each fidelity term similar values of PSNR and $\|\mathbf{x}_*\|_1$ can be obtained for different values of β . Yet, as shown in Figs. 3b, different values of β significantly change the convergence rate of FISTA for the same fidelity term (a known behavior for proximal methods, see, e.g., (Hale et al., 2008)). Therefore, contrary to our conclusion for PGD, in this case, when β is uniformly tuned for best PSNR of each fidelity term, an “extrinsic source”

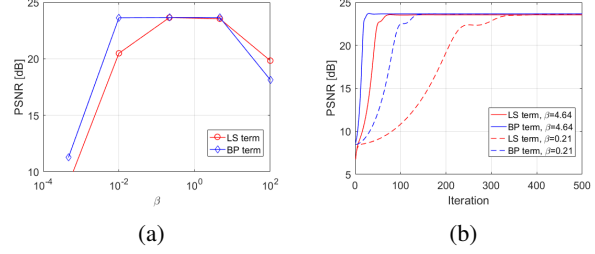


Figure 3: Compressed sensing with $m/n = 0.5$ Gaussian measurements and SNR of 20dB. PSNR (averaged over 4 test images) of FISTA with ℓ_1 prior versus: (a) regularization parameter β (for 1000 iterations); (b) iteration number (for $\beta = 0.21, 4.64$).

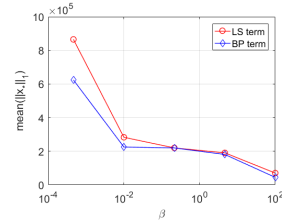


Figure 4: Average $\|\mathbf{x}_*\|_1$ for the recoveries from Fig. 3a vs. β .

(β setting) can affect the convergence rate as well.

Finally, we emphasize that, in general, having $\beta_{BP} \neq \beta_{LS}$ in a penalized formulation *does not* have an immediate implication on the different convergence rates of proximal methods (e.g., $\beta_{BP} > \beta_{LS}$ does not necessarily imply that in the equivalent constrained formulations $R_{BP} < R_{LS}$). This is mainly because the scale of $\ell_{LS}(\tilde{\mathbf{x}})$ and $\ell_{BP}(\tilde{\mathbf{x}})$ may be very different (depends on \mathbf{A}^\dagger in the problem).

5.2. DCGAN Prior

In the recent years there has been a significant improvement in learning generative models via deep neural networks. Methods like variational auto-encoders (VAEs) (Kingma & Welling, 2013) and generative adversarial networks (GANs) (Goodfellow et al., 2014) have found success at modeling data distributions. This has naturally led to using pre-trained generative models as priors in imaging inverse problems (see, e.g., (Bora et al., 2017; Shah & Hegde, 2018; Abu Hussein et al., 2020)).

Since in popular generative models (Kingma & Welling, 2013; Goodfellow et al., 2014) a generator $\mathcal{G}(\cdot)$ learns a mapping from a low dimensional space $\mathbf{z} \in \mathbb{R}^d$ to the signal space $\mathcal{G}(\mathbf{z}) \subset \mathbb{R}^n$ ($d \ll n$), one can search for a reconstruction of \mathbf{x} only in the range of a pre-trained generator, i.e., in the set $\mathcal{K} = \{\tilde{\mathbf{x}} \in \mathbb{R}^n : \exists \mathbf{z} \in \mathbb{R}^d \text{ s.t. } \tilde{\mathbf{x}} = \mathcal{G}(\mathbf{z})\}$. Note that the proposed PGD theory, which assumes in (9) that $\mathcal{K} = \{\tilde{\mathbf{x}} \in \mathbb{R}^n : s(\tilde{\mathbf{x}}) \leq R\}$, covers the above feasible set

for $R = 0$ and the following non-convex prior

$$s(\tilde{\mathbf{x}}) = \begin{cases} 0, & \exists \tilde{\mathbf{z}} \in \mathbb{R}^d : \tilde{\mathbf{x}} = \mathcal{G}(\tilde{\mathbf{z}}) \\ +\infty, & \text{otherwise} \end{cases}. \quad (31)$$

In the next experiments we use $\mathcal{G}(\mathbf{z})$ that we obtained by training a DCGAN (Radford et al., 2015) on the first 200,000 images (out of 202,599) of CelebA dataset. We use the 64×64 version of the images (so $n = 64^2$) and a training procedure similar to (Radford et al., 2015; Bora et al., 2017).

We start with the CS scenario from previous section, where $m/n = 0.5$, the entries of the measurement matrix are i.i.d. drawn from $\mathcal{N}(0, 1/m)$, and the SNR is 20dB. The last 10 images in CelebA are used as test images.

The recovery using each of the LS and BP objectives is based on 50 iterations of PGD with the typical step-size of 1 over the spectral norm of the objective’s Hessian, and initialization of $\tilde{\mathbf{x}}_0 = \mathbf{A}^\dagger \mathbf{y}$. As the projection $\mathcal{P}_{\mathcal{K}}(\tilde{\mathbf{x}})$ we use $\mathcal{G}(\tilde{\mathbf{z}})$, where $\tilde{\mathbf{z}}$ is obtained by minimizing $\|\tilde{\mathbf{x}} - \mathcal{G}(\tilde{\mathbf{z}})\|_2^2$ with respect to $\tilde{\mathbf{z}}$. This inner (non-convex) minimization problem is carried out by 1000 iterations of ADAM (Kingma & Ba, 2014) with learning rate of 0.1 and multiple initializations. The value of $\tilde{\mathbf{z}}$ that gives the lowest $\|\tilde{\mathbf{x}} - \mathcal{G}(\tilde{\mathbf{z}})\|_2^2$ is chosen as $\hat{\mathbf{z}}$. For the projection in the first PGD iteration we use the same 10 random initializations of $\tilde{\mathbf{z}}$ for both LS and BP. For the other PGD iterations, warm starts are used (i.e., values of $\tilde{\mathbf{z}}$ from the end of the inner minimization in previous iteration). For both LS and BP objectives the computational cost of a PGD iteration is dominated by the complexity of the projection. Thus, the overall complexity for each objective is dictated by the number of iterations that it requires.

Table 1 shows the PSNR of the reconstructions, averaged over the test images. Several visual results are shown in Fig. 5. Fig. 6a shows the average PSNR as a function of the iteration number. Again, it is clear that BP objective requires significantly fewer iterations. Since the DCGAN prior does not require a regularization parameter, the discussed “extrinsic” source of faster convergence is not relevant. However, recall that DCGAN prior is (highly) non-convex, contrary to the ℓ_1 -norm prior. Therefore, \mathbf{x}_*^{LS} and \mathbf{x}_*^{BP} , the PGD stationary points for LS and BP objectives, may be extremely different, and similarly, their two associated cones $\mathcal{C}_s(\mathbf{x}_*^{LS})$ and $\mathcal{C}_s(\mathbf{x}_*^{BP})$ may have very different geometries. This fact is another source for different convergence rates.

As an attempt to (approximately) isolate the effect of the intrinsic source on the convergence rates, we present in Fig. 6b the PSNR vs. iteration number only for image 202592 in CelebA, where the recoveries using LS and BP objectives are relatively similar (see Fig. 5). The similarity between the convergence rates in Figs. 6a and 6b hints that the inherent advantage of BP plays an essential role in its faster PGD convergence also for the other images in the examined

Table 1: PSNR [dB] (averaged over 10 test images) of PGD with 50 iterations and DCGAN prior for: (a) CS with $m/n = 0.5$ Gaussian measurements and SNR of 20dB; (b) SR with Gaussian filter and scale factor of 3.

	LS objective	BP objective
CS $m/n = 0.5$	23.14	23.57
SR x3	23.29	23.90

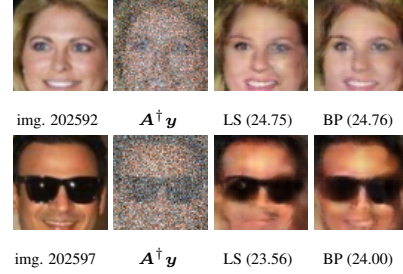


Figure 5: CS with $m/n = 0.5$ Gaussian measurements and SNR of 20dB, using PGD with 50 iterations and DCGAN prior.

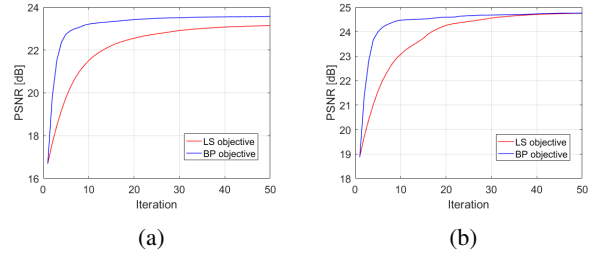


Figure 6: Compressed sensing with $m/n = 0.5$ Gaussian measurements and SNR of 20dB. PSNR of PGD with DCGAN prior versus the iteration number: (a) averaged over 10 CelebA test images; (b) for image 202592 in CelebA.

scenario, where the recoveries are not similar.

Our final experiment demonstrates faster PGD convergence of BP objective for a different observation model—the SR task, where \mathbf{A} is a composite operator of anti-aliasing filtering followed by down-sampling. We consider a commonly examined scenario with scale factor of 3 and Gaussian filter of size 7×7 and standard deviation 1.6. For the reconstruction, we use PGD with DCGAN prior, initialized with bicubic upsampling of \mathbf{y} . The rest of the configuration is exactly as used for CS (obviously, now the gradients and the step-size are computed for the new relevant \mathbf{A}).

Table 1 shows the PSNR of the reconstructions, averaged over the test images. Several visual results are shown in Fig. 7. Fig. 8 shows the average PSNR versus the iteration number. Once again, the convergence of PGD for the BP objective is faster. However, this time the difference in the convergence rates is modest. Since in this SR experiment we have obtained significantly different recoveries for the

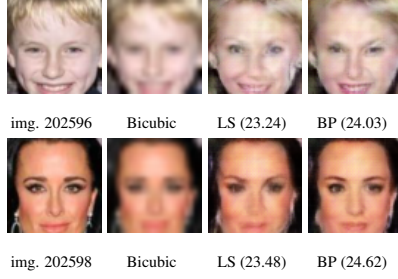


Figure 7: SR with Gaussian filter and scale factor of 3, using PGD with 50 iterations and DCGAN prior.

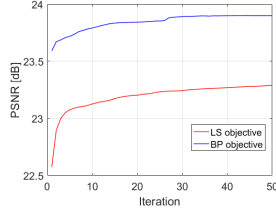


Figure 8: Super-resolution with Gaussian filter and scale factor of 3. PSNR (averaged over 10 test images) of PGD with DCGAN prior versus the iteration number.

LS and BP objectives (BP consistently yields higher PSNR), we cannot try to isolate the effect of the intrinsic source, as done above. Yet, presumably in this SR scenario the prior imposes a weaker restriction on the null space of \mathbf{A} than in the CS scenario above, which is translated in the analysis to a smaller gap between $P_{LS}(\mathcal{C}_s(\mathbf{x}_*))$ and $P_{BP}(\mathcal{C}_s(\mathbf{x}_*))$.

6. Conclusion

In this paper we compared the convergence rate of PGD applied on LS and BP objectives, and identified an *intrinsic* source of a faster convergence for BP. Numerical experiments supported our theoretical findings for both convex (ℓ_1 -norm) and non-convex (pre-trained DCGAN) priors. For the ℓ_1 -norm prior, we also provided numerical experiments that connected the PGD analysis with the behavior observed for proximal gradient method in (Tirer & Giryes, 2020). A study of the latter has further highlighted the advantage of BP over LS when $\mathbf{A}\mathbf{A}^T$ is badly conditioned.

A possible direction for future research is obtaining a lower bound for $\inf_{\mathbf{u} \in \mathcal{C}_s(\mathbf{x}_*) \cap \mathbb{S}^{n-1}} \|(\mathbf{A}\mathbf{A}^T)^{-\frac{1}{2}} \mathbf{A}\mathbf{u}\|_2^2$, which is tighter than $\sigma_{\min}((\mathbf{A}\mathbf{A}^T)^{-1}) \inf_{\mathbf{u} \in \mathcal{C}_s(\mathbf{x}_*) \cap \mathbb{S}^{n-1}} \|\mathbf{A}\mathbf{u}\|_2^2$ in certain cases. This will directly imply a *strict* advantage of the BP objective in Proposition 3.4 in these cases. The difficulty of obtaining such a theoretical result for Gaussian \mathbf{A} and sparsity priors is discussed in Section 3. Yet, the experiments in this paper consistently demonstrate that such a strict advantage of BP exists.

Acknowledgment. The authors would like to thank Amir Beck for fruitful discussions. This research is supported by ERC-StG grant no. 757497 (SPADE) and gifts from NVIDIA, Amazon, and Google.

References

- Abu Hussein, S., Tirer, T., and Giryes, R. Image-adaptive GAN based reconstruction. *AAAI Conference on Artificial Intelligence*, 2020.
- Amelunxen, D., Lotz, M., McCoy, M. B., and Tropp, J. A. Living on the edge: Phase transitions in convex programs with random data. *Information and Inference: A Journal of the IMA*, 3(3):224–294, 2014.
- Beck, A. *First-order methods in optimization*, volume 25. SIAM, 2017.
- Beck, A. and Teboulle, M. A fast iterative shrinkage-thresholding algorithm for linear inverse problems. *SIAM journal on imaging sciences*, 2(1):183–202, 2009.
- Bora, A., Jalal, A., Price, E., and Dimakis, A. G. Compressed sensing using generative models. In *Proceedings of the 34th International Conference on Machine Learning-Volume 70*, pp. 537–546. JMLR. org, 2017.
- Candès, E. J. and Wakin, M. B. An introduction to compressive sampling. *IEEE signal processing magazine*, 25(2): 21–30, 2008.
- Chandrasekaran, V., Recht, B., Parrilo, P. A., and Willsky, A. S. The convex geometry of linear inverse problems. *Foundations of Computational mathematics*, 12(6):805–849, 2012.
- Danielyan, A., Katkovnik, V., and Egiazarian, K. BM3D frames and variational image deblurring. *IEEE Transactions on Image Processing*, 21(4):1715–1728, 2012.
- Donoho, D. L. Compressed sensing. *IEEE Transactions on information theory*, 52(4):1289–1306, 2006.
- Duchi, J., Shalev-Shwartz, S., Singer, Y., and Chandra, T. Efficient projections onto the ℓ_1 -ball for learning in high dimensions. In *Proceedings of the 25th international conference on Machine learning*, pp. 272–279. ACM, 2008.
- Genzel, M., Kutyniok, G., and März, M. ℓ_1 -analysis minimization and generalized (co-) sparsity: When does recovery succeed? *arXiv preprint arXiv:1710.04952*, 2017.
- Goodfellow, I., Pouget-Abadie, J., Mirza, M., Xu, B., Warde-Farley, D., Ozair, S., Courville, A., and Bengio, Y. Generative adversarial nets. In *Advances in neural information processing systems*, pp. 2672–2680, 2014.

- Gordon, Y. On Milman's inequality and random subspaces which escape through a mesh in \mathbb{R}^n . In *Geometric Aspects of Functional Analysis*, pp. 84–106. Springer, 1988.
- Hale, E. T., Yin, W., and Zhang, Y. Fixed-point continuation for ℓ_1 -minimization: Methodology and convergence. *SIAM Journal on Optimization*, 19(3):1107–1130, 2008.
- Kingma, D. P. and Ba, J. Adam: A method for stochastic optimization. *arXiv preprint arXiv:1412.6980*, 2014.
- Kingma, D. P. and Welling, M. Auto-encoding variational bayes. *arXiv preprint arXiv:1312.6114*, 2013.
- Moreau, J.-J. Proximité et dualité dans un espace hilbertien. *Bull. Soc. Math. France*, 93(2):273–299, 1965.
- Oymak, S., Recht, B., and Soltanolkotabi, M. Sharp time–data tradeoffs for linear inverse problems. *IEEE Transactions on Information Theory*, 64(6):4129–4158, 2017.
- Plan, Y. and Vershynin, R. Robust 1-bit compressed sensing and sparse logistic regression: A convex programming approach. *IEEE Transactions on Information Theory*, 59(1):482–494, 2012.
- Radford, A., Metz, L., and Chintala, S. Unsupervised representation learning with deep convolutional generative adversarial networks. *arXiv preprint arXiv:1511.06434*, 2015.
- Rudin, L. I., Osher, S., and Fatemi, E. Nonlinear total variation based noise removal algorithms. *Physica D: nonlinear phenomena*, 60(1-4):259–268, 1992.
- Shah, V. and Hegde, C. Solving linear inverse problems using gan priors: An algorithm with provable guarantees. In *2018 IEEE International Conference on Acoustics, Speech and Signal Processing (ICASSP)*, pp. 4609–4613. IEEE, 2018.
- Teodoro, A. M., Bioucas-Dias, J. M., and Figueiredo, M. A. A convergent image fusion algorithm using scene-adapted gaussian-mixture-based denoising. *IEEE Transactions on Image Processing*, 28(1):451–463, 2018.
- Tikhonov, A. N. On the solution of ill-posed problems and the method of regularization. In *Doklady Akademii Nauk*, volume 151, pp. 501–504. Russian Academy of Sciences, 1963.
- Tirer, T. and Giryes, R. Image restoration by iterative denoising and backward projections. *IEEE Transactions on Image Processing*, 28(3):1220–1234, 2018.
- Tirer, T. and Giryes, R. Super-resolution via image-adapted denoising CNNs: Incorporating external and internal learning. *IEEE Signal Processing Letters*, 26(7):1080–1084, 2019.
- Tirer, T. and Giryes, R. Back-projection based fidelity term for ill-posed linear inverse problems. *IEEE Transactions on Image Processing*, 2020.
- Yang, J., Wright, J., Huang, T. S., and Ma, Y. Image super-resolution via sparse representation. *IEEE transactions on image processing*, 19(11):2861–2873, 2010.

A. Proof of Theorem 3.1

In this section we prove Theorem 3.1. To this end we adopt the following three lemmas from (Oymak et al., 2017) (numbered there as Lemmas 16–18).

Lemma A.1. *Let $\mathcal{C} \subset \mathbb{R}^n$ be a closed cone and $\mathbf{v} \in \mathbb{R}^n$. Then*

$$\|\mathcal{P}_{\mathcal{C}}(\mathbf{v})\|_2 = \sup_{\mathbf{v} \in \mathcal{C} \cap \mathbb{B}^n} \mathbf{u}^T \mathbf{v}. \quad (32)$$

Lemma A.2. *Let $\mathcal{K} \subset \mathbb{R}^n$ be a closed set and $\mathbf{u}, \mathbf{v} \in \mathbb{R}^n$. The projection onto \mathcal{K} obeys*

$$\mathcal{P}_{\mathcal{K}}(\mathbf{u} + \mathbf{v}) - \mathbf{u} = \mathcal{P}_{\mathcal{K}-\mathbf{u}}(\mathbf{v}). \quad (33)$$

Lemma A.3. *Let \mathcal{D} and \mathcal{C} be a nonempty and closed set and a closed cone, respectively, such that $\mathbf{0} \in \mathcal{D}$ and $\mathcal{D} \subseteq \mathcal{C}$. Then for all $\mathbf{v} \in \mathbb{R}^n$*

$$\|\mathcal{P}_{\mathcal{D}}(\mathbf{v})\|_2 \leq \kappa \|\mathcal{P}_{\mathcal{C}}(\mathbf{v})\|_2, \quad (34)$$

where $\kappa = 1$ if \mathcal{D} is a convex set and $\kappa = 2$ otherwise.

Let us now prove Theorem 3.1. Since $s(\mathbf{x}_*) = R$, we have that $\tilde{\mathbf{x}}_t - \mathbf{x}_*$ is inside the descent set $\mathcal{D}_s(\mathbf{x}_*)$ for all t . For simplicity let us define $\mathcal{D} \triangleq \mathcal{D}_s(\mathbf{x}_*)$ and $\mathcal{C} \triangleq \mathcal{C}_s(\mathbf{x}_*)$. We obtain (17) by

$$\begin{aligned} \|\tilde{\mathbf{x}}_{t+1} - \mathbf{x}_*\|_2 &= \|\mathcal{P}_{\mathcal{K}}(\tilde{\mathbf{x}}_t + \mu \mathbf{W}(\mathbf{y} - \mathbf{A}\tilde{\mathbf{x}}_t)) - \mathbf{x}_*\|_2 \\ &\stackrel{(a)}{=} \|\mathcal{P}_{\mathcal{K}-\mathbf{x}_*}(\tilde{\mathbf{x}}_t + \mu \mathbf{W}(\mathbf{y} - \mathbf{A}\tilde{\mathbf{x}}_t) - \mathbf{x}_*)\|_2 \\ &\stackrel{(b)}{=} \|\mathcal{P}_{\mathcal{D}}(\tilde{\mathbf{x}}_t + \mu \mathbf{W}(\mathbf{y} - \mathbf{A}\tilde{\mathbf{x}}_t) - \mathbf{x}_*)\|_2 \\ &\stackrel{(c)}{\leq} \kappa_s \|\mathcal{P}_{\mathcal{C}}(\tilde{\mathbf{x}}_t + \mu \mathbf{W}(\mathbf{y} - \mathbf{A}\tilde{\mathbf{x}}_t) - \mathbf{x}_*)\|_2 \\ &= \kappa_s \|\mathcal{P}_{\mathcal{C}}((\mathbf{I}_n - \mu \mathbf{W}\mathbf{A})(\tilde{\mathbf{x}}_t - \mathbf{x}_*) + \mu \mathbf{W}(\mathbf{y} - \mathbf{A}\mathbf{x}_*))\|_2 \\ &\stackrel{(d)}{=} \kappa_s \sup_{\mathbf{v} \in \mathcal{C} \cap \mathbb{B}^n} \mathbf{v}^T [(\mathbf{I}_n - \mu \mathbf{W}\mathbf{A})(\tilde{\mathbf{x}}_t - \mathbf{x}_*) + \mu \mathbf{W}(\mathbf{y} - \mathbf{A}\mathbf{x}_*)] \\ &\leq \kappa_s \sup_{\mathbf{v} \in \mathcal{C} \cap \mathbb{B}^n} \mathbf{v}^T (\mathbf{I}_n - \mu \mathbf{W}\mathbf{A})(\tilde{\mathbf{x}}_t - \mathbf{x}_*) + \kappa_s \mu \xi(\mathcal{C}) \\ &\stackrel{(e)}{\leq} \kappa_s \rho(\mathcal{C}) \|\tilde{\mathbf{x}}_t - \mathbf{x}_*\|_2 + \kappa_s \mu \xi(\mathcal{C}), \end{aligned} \quad (35)$$

where (a) follows from Lemma A.2, (b) follows from plugging $R = s(\mathbf{x}_*)$ in the definition of \mathcal{K} (given in (9)), (c) follows from Lemma A.3, (d) follows from Lemma A.1, and (e) follows from $\tilde{\mathbf{x}}_t - \mathbf{x}_* \in \mathcal{D} \subseteq \mathcal{C}$.

B. Results for Proximal Gradient Method Under a Relaxed Contractive Assumption

In this section we show that given a certain contractive condition it is possible to identify an advantage in the convergence rate of the BP term over the LS term directly for the proximal gradient method. Yet, as discussed in Section 4, in the main body of the paper we mainly focus on the PGD results for two reasons. Firstly, the PGD results do not require a contractive assumption, but rather very mild assumptions (except of a step-size assumption that is inevitable if one wants to ensure convergence for a *constant* step-size). Secondly, identifying an “intrinsic factor” for different convergence rates is easier for PGD because, as shown below, the dependence of the results in this section on β_{LS}, β_{BP} is not clear, and the effect of these regularization parameters cannot be bypassed by assuming $\mathbf{x}_*^{LS} \approx \mathbf{x}_*^{BP}$, as done in Section 3.3 for the regularization parameters in PGD.

To proceed, let us present the proximal mapping, which was introduced in (Moreau, 1965), and the proximal gradient method that is used to solve the unconstrained optimization problem (2).

Definition B.1. *The proximal mapping of a convex function $s(\cdot)$ at the point $\tilde{\mathbf{z}}$ is defined by*

$$\text{prox}_{s(\cdot)}(\tilde{\mathbf{z}}) \triangleq \underset{\tilde{\mathbf{x}}}{\text{argmin}} \frac{1}{2} \|\tilde{\mathbf{z}} - \tilde{\mathbf{x}}\|_2^2 + s(\tilde{\mathbf{x}}). \quad (36)$$

Assuming a differentiable fidelity term $\ell(\tilde{\mathbf{x}})$ with a Lipschitz continuous gradient $\nabla \ell(\tilde{\mathbf{x}})$, applying proximal gradient method (often referred to as ISTA) on (2) involves iterations of

$$\tilde{\mathbf{x}}_{t+1} = \text{prox}_{\mu\beta s(\cdot)}(\tilde{\mathbf{x}}_t - \mu \nabla \ell(\tilde{\mathbf{x}}_t)), \quad (37)$$

where μ is a step-size, which ensures sublinear convergence for convex $s(\cdot)$ if it is equal to (or smaller than) 1 over the Lipschitz constant of $\nabla \ell(\tilde{\mathbf{x}})$ (Beck & Teboulle, 2009).

Note that the proximal mapping of any convex $\beta s(\cdot)$ is non-expansive (see, e.g., (Beck, 2017)), i.e.,

$$\|\text{prox}_{\beta s(\cdot)}(\tilde{\mathbf{z}}_1) - \text{prox}_{\beta s(\cdot)}(\tilde{\mathbf{z}}_2)\|_2 \leq \|\tilde{\mathbf{z}}_1 - \tilde{\mathbf{z}}_2\|_2 \quad \forall \tilde{\mathbf{z}}_1, \tilde{\mathbf{z}}_2. \quad (38)$$

This property is not enough to obtain an expression that allows to distinguish between the convergence rates of LS and BP (as done using (17) for PGD). Therefore, more assumptions/conditions on $\beta s(\cdot)$ are required. One such condition on $\beta s(\cdot)$ is that its proximal mapping is a contraction, i.e., there exists $0 \leq k_{\beta s(\cdot)} < 1$ such that

$$\|\text{prox}_{\beta s(\cdot)}(\tilde{\mathbf{z}}_1) - \text{prox}_{\beta s(\cdot)}(\tilde{\mathbf{z}}_2)\|_2 \leq k_{\beta s(\cdot)} \|\tilde{\mathbf{z}}_1 - \tilde{\mathbf{z}}_2\|_2 \quad \forall \tilde{\mathbf{z}}_1, \tilde{\mathbf{z}}_2. \quad (39)$$

Note that even though the above condition is rather strict, it is satisfied by some prior functions such as Tikhonov regularization (Tikhonov, 1963) (where $s(\tilde{\mathbf{x}}) = \frac{1}{2} \|\mathbf{D}\tilde{\mathbf{x}}\|_2^2$ and $\mathbf{D}^T \mathbf{D}$ is positive definite) or even a recent GMM-based prior (Teodoro et al., 2018) (see Lemma 2 there). Yet, for the main result of this section we require a condition that is less demanding than (39).

Our result requires a relaxed contraction condition that ties the prior $\beta s(\cdot)$ with the measurement matrix \mathbf{A} . Namely, it requires that the proximal mapping of $\beta s(\cdot)$ is a contraction *only* in the null space of \mathbf{A} .

Condition B.2. *Given the convex function $\beta s(\cdot)$ and the full row-rank matrix \mathbf{A} , there exists $0 < \sigma_{\mathbf{A}, \beta s(\cdot)} \leq 1$ such that*

$$\|\text{prox}_{\beta s(\cdot)}(\tilde{\mathbf{z}}_1) - \text{prox}_{\beta s(\cdot)}(\tilde{\mathbf{z}}_2)\|_2 \leq \|(\mathbf{P}_A + (1 - \sigma_{\mathbf{A}, \beta s(\cdot)})\mathbf{Q}_A)(\tilde{\mathbf{z}}_1 - \tilde{\mathbf{z}}_2)\|_2 \quad \forall \tilde{\mathbf{z}}_1, \tilde{\mathbf{z}}_2, \quad (40)$$

where $\mathbf{Q}_A \triangleq \mathbf{I}_n - \mathbf{P}_A$ and $\mathbf{P}_A \triangleq \mathbf{A}^\dagger \mathbf{A}$ are the orthogonal projections onto the null space of \mathbf{A} and the row space of \mathbf{A} , respectively.

Note that satisfying (39) with $k_{\beta s(\cdot)}$ implies satisfying (40) with $\sigma_{\mathbf{A}, \beta s(\cdot)} = 1 - k_{\beta s(\cdot)}$. This is a simple consequence of the Pythagorean theorem and the fact that $0 \leq k_{\beta s(\cdot)} < 1$

$$\begin{aligned} \|\text{prox}_{\beta s(\cdot)}(\tilde{\mathbf{z}}_1) - \text{prox}_{\beta s(\cdot)}(\tilde{\mathbf{z}}_2)\|_2^2 &\leq k_{\beta s(\cdot)}^2 \|\tilde{\mathbf{z}}_1 - \tilde{\mathbf{z}}_2\|_2^2 \\ &= k_{\beta s(\cdot)}^2 (\|\mathbf{P}_A(\tilde{\mathbf{z}}_1 - \tilde{\mathbf{z}}_2)\|_2^2 + \|\mathbf{Q}_A(\tilde{\mathbf{z}}_1 - \tilde{\mathbf{z}}_2)\|_2^2) \\ &\leq \|\mathbf{P}_A(\tilde{\mathbf{z}}_1 - \tilde{\mathbf{z}}_2)\|_2^2 + \|k_{\beta s(\cdot)} \mathbf{Q}_A(\tilde{\mathbf{z}}_1 - \tilde{\mathbf{z}}_2)\|_2^2 \\ &= \|(\mathbf{P}_A + k_{\beta s(\cdot)} \mathbf{Q}_A)(\tilde{\mathbf{z}}_1 - \tilde{\mathbf{z}}_2)\|_2^2. \end{aligned} \quad (41)$$

The constant $\sigma_{\mathbf{A}, \beta s(\cdot)}$ in Condition B.2 measures the restriction that the prior $\beta s(\cdot)$ imposes on the null space of \mathbf{A} . For the restrictive prior (12), given in the warm-up Section 3.1, it is easy to see that $\text{prox}_{\beta s_{\text{oracle}}(\cdot)}(\tilde{\mathbf{z}}) = \mathbf{P}_A \tilde{\mathbf{z}} + \mathbf{Q}_A \mathbf{x}$, which implies $\sigma_{\mathbf{A}, \beta s_{\text{oracle}}(\cdot)} = 1$. On the other hand, the general property in (38) is obtained for $\sigma_{\mathbf{A}, \beta s(\cdot)} = 0$ (because $\mathbf{P}_A + \mathbf{Q}_A = \mathbf{I}_n$). Furthermore, note that for $\beta_1 \geq \beta_2$ we have that the weight of the prior $s(\cdot)$ in (36) is larger for $\text{prox}_{\beta_1 s(\cdot)}(\tilde{\mathbf{z}})$ than for $\text{prox}_{\beta_2 s(\cdot)}(\tilde{\mathbf{z}})$. Therefore, it is expected to impose a stronger restriction on the null space of \mathbf{A} , or equivalently $\sigma_{\mathbf{A}, \beta_1 s(\cdot)} \geq \sigma_{\mathbf{A}, \beta_2 s(\cdot)}$.

The following theorem shows that if Condition B.2 holds, then the iterates (37) exhibit a linear convergence under certain conditions that are satisfied by both $\ell_{LS}(\tilde{\mathbf{x}})$ and $\ell_{BP}(\tilde{\mathbf{x}})$.

Theorem B.3. *Consider the penalized optimization problem (2) with convex $s(\cdot)$ and twice differentiable convex $\ell(\cdot)$ that satisfies $\nabla \ell(\cdot) \in \text{range}(\mathbf{A}^T)$ for a given full row-rank matrix \mathbf{A} . Denote by $\tilde{\sigma}_{\max}$ the largest eigenvalue of $\nabla^2 \ell$ and by $\tilde{\sigma}_{\min}$ the smallest non-zero eigenvalue of $\nabla^2 \ell$. Then, if Condition B.2 holds for $\mu\beta s(\cdot)$ and \mathbf{A} , we have that the sequence $\{\tilde{\mathbf{x}}_t\}$ obtained by (37) with $\mu = 1/\tilde{\sigma}_{\max}$ converges to a point \mathbf{x}_* and obeys*

$$\|\tilde{\mathbf{x}}_{t+1} - \mathbf{x}_*\|_2 \leq \max \left\{ 1 - \frac{\tilde{\sigma}_{\min}}{\tilde{\sigma}_{\max}}, 1 - \sigma_{\mathbf{A}, \frac{\beta}{\tilde{\sigma}_{\max}} s(\cdot)} \right\} \|\tilde{\mathbf{x}}_t - \mathbf{x}_*\|_2. \quad (42)$$

Proof. The existence of the stationary point $\mathbf{x}_* = \text{prox}_{\mu\beta s(\cdot)}(\mathbf{x}_* - \mu\nabla\ell(\mathbf{x}_*))$ (that is a minimizer of (2)) to which proximal gradient descent with step-size $\mu = 1/\tilde{\sigma}_{max}$ converges follows from the theory in (Beck & Teboulle, 2009). Yet, this result guarantees only sub-linear convergence. In the following we obtain the desired linear convergence result.

$$\begin{aligned}
 \|\tilde{\mathbf{x}}_{t+1} - \mathbf{x}_*\|_2 &= \|\text{prox}_{\mu\beta s(\cdot)}(\tilde{\mathbf{x}}_t - \mu\nabla\ell(\tilde{\mathbf{x}}_t)) - \text{prox}_{\mu\beta s(\cdot)}(\mathbf{x}_* - \mu\nabla\ell(\mathbf{x}_*))\|_2 \\
 &\stackrel{(a)}{\leq} \|(\mathbf{P}_A + (1 - \sigma_{\mathbf{A}, \mu\beta s(\cdot)})\mathbf{Q}_A)((\tilde{\mathbf{x}}_t - \mu\nabla\ell(\tilde{\mathbf{x}}_t)) - (\mathbf{x}_* - \mu\nabla\ell(\mathbf{x}_*)))\|_2 \\
 &\stackrel{(b)}{=} \|((\mathbf{P}_A + (1 - \sigma_{\mathbf{A}, \mu\beta s(\cdot)})\mathbf{Q}_A)\tilde{\mathbf{x}}_t - \mu\nabla\ell(\tilde{\mathbf{x}}_t)) - ((\mathbf{P}_A + (1 - \sigma_{\mathbf{A}, \mu\beta s(\cdot)})\mathbf{Q}_A)\mathbf{x}_* - \mu\nabla\ell(\mathbf{x}_*))\|_2 \\
 &\stackrel{(c)}{=} \|\mathbf{g}(\tilde{\mathbf{x}}_t) - \mathbf{g}(\mathbf{x}_*)\|_2,
 \end{aligned} \tag{43}$$

where (a) follows from Condition B.2 and (b) follows from the fact that $\nabla\ell(\cdot) \in \text{range}(\mathbf{A}^T)$, which implies $\mathbf{P}_A\nabla\ell(\cdot) = \nabla\ell(\cdot)$ and $\mathbf{Q}_A\nabla\ell(\cdot) = 0$, and (c) uses the definition $\mathbf{g}(\tilde{\mathbf{x}}) \triangleq (\mathbf{P}_A + (1 - \sigma_{\mathbf{A}, \mu\beta s(\cdot)})\mathbf{Q}_A)\tilde{\mathbf{x}} - \mu\nabla\ell(\tilde{\mathbf{x}})$.

Using Taylor series expansion consideration, there exists a point $\tilde{\boldsymbol{\xi}}$ in the ray between $\tilde{\mathbf{x}}_t$ and \mathbf{x}_* , such that $\|\mathbf{g}(\tilde{\mathbf{x}}_t) - \mathbf{g}(\mathbf{x}_*)\|_2 = \|\nabla\mathbf{g}(\tilde{\boldsymbol{\xi}})(\tilde{\mathbf{x}}_t - \mathbf{x}_*)\|_2$. Therefore,

$$\|\mathbf{g}(\tilde{\mathbf{x}}_t) - \mathbf{g}(\mathbf{x}_*)\|_2 \leq \|\nabla\mathbf{g}(\tilde{\boldsymbol{\xi}})\| \|\tilde{\mathbf{x}}_t - \mathbf{x}_*\|_2 \leq \max_{\tilde{\boldsymbol{\xi}}} \|\nabla\mathbf{g}(\tilde{\boldsymbol{\xi}})\| \|\tilde{\mathbf{x}}_t - \mathbf{x}_*\|_2, \tag{44}$$

which yields

$$\|\tilde{\mathbf{x}}_{t+1} - \mathbf{x}_*\|_2 \leq \max_{\tilde{\boldsymbol{\xi}}} \|\nabla\mathbf{g}(\tilde{\boldsymbol{\xi}})\| \|\tilde{\mathbf{x}}_t - \mathbf{x}_*\|_2. \tag{45}$$

Note that $\nabla\mathbf{g}(\tilde{\mathbf{x}}) = \mathbf{P}_A - \mu\nabla^2\ell(\tilde{\mathbf{x}}) + (1 - \sigma_{\mathbf{A}, \mu\beta s(\cdot)})\mathbf{Q}_A$. Therefore, we have $\max_{\tilde{\boldsymbol{\xi}}} \|\nabla\mathbf{g}(\tilde{\boldsymbol{\xi}})\| = \max\{|1 - \mu\tilde{\sigma}_{max}|, |1 - \mu\tilde{\sigma}_{min}|, 1 - \sigma_{\mathbf{A}, \mu\beta s(\cdot)}\}$. Recall that $\tilde{\sigma}_{max}$ is the largest eigenvalue of $\nabla^2\ell(\cdot)$ and $\tilde{\sigma}_{min}$ is the smallest *non-zero* eigenvalue of $\nabla^2\ell(\cdot)$. Note that $\max_{\tilde{\boldsymbol{\xi}}} \|\nabla\mathbf{g}(\tilde{\boldsymbol{\xi}})\|$ dictates the convergence rate (i.e., “the smaller the better”, and if it equals 1 then convergence is not guaranteed). A common choice of step-size that well handles the first two terms is $\mu = 1/\tilde{\sigma}_{max}$, which leads to $\max_{\tilde{\boldsymbol{\xi}}} \|\nabla\mathbf{g}(\tilde{\boldsymbol{\xi}})\| = \max\left\{0, 1 - \frac{\tilde{\sigma}_{min}}{\tilde{\sigma}_{max}}, 1 - \sigma_{\mathbf{A}, \frac{\beta}{\tilde{\sigma}_{max}}s(\cdot)}\right\}$ and completes the proof. \square

For LS we have $\nabla\ell_{LS}(\tilde{\mathbf{x}}) = -\mathbf{A}^T(\mathbf{y} - \mathbf{A}\tilde{\mathbf{x}})$ and $\nabla^2\ell_{LS}(\tilde{\mathbf{x}}) = \mathbf{A}^T\mathbf{A}$. Therefore, $\tilde{\sigma}_{max} = \sigma_{max}(\mathbf{A}\mathbf{A}^T)$ and $\tilde{\sigma}_{min} = \sigma_{min}(\mathbf{A}\mathbf{A}^T)$, and Theorem B.3 implies

$$\|\tilde{\mathbf{x}}_{t+1}^{LS} - \mathbf{x}_*^{LS}\|_2 \leq \max\left\{1 - \frac{\sigma_{min}(\mathbf{A}\mathbf{A}^T)}{\sigma_{max}(\mathbf{A}\mathbf{A}^T)}, 1 - \sigma_{\mathbf{A}, \frac{\beta_{LS}}{\sigma_{max}(\mathbf{A}\mathbf{A}^T)}s(\cdot)}\right\} \|\tilde{\mathbf{x}}_t^{LS} - \mathbf{x}_*^{LS}\|_2. \tag{46}$$

For BP we have $\nabla\ell_{BP}(\tilde{\mathbf{x}}) = -\mathbf{A}^\dagger(\mathbf{y} - \mathbf{A}\tilde{\mathbf{x}})$ and $\nabla^2\ell_{BP}(\tilde{\mathbf{x}}) = \mathbf{A}^\dagger\mathbf{A}$. Therefore, $\tilde{\sigma}_{max} = 1$ and $\tilde{\sigma}_{min} = 1$, and Theorem B.3 implies

$$\|\tilde{\mathbf{x}}_{t+1}^{BP} - \mathbf{x}_*^{BP}\|_2 \leq (1 - \sigma_{\mathbf{A}, \beta_{BP}s(\cdot)}) \|\tilde{\mathbf{x}}_t^{BP} - \mathbf{x}_*^{BP}\|_2. \tag{47}$$

Comparing (46) and (47) we conclude that if Condition B.2 holds, then the proximal gradient method on $\ell_{BP}(\tilde{\mathbf{x}}) + \beta_{BP}s(\tilde{\mathbf{x}})$ is faster than on $\ell_{LS}(\tilde{\mathbf{x}}) + \beta_{LS}s(\tilde{\mathbf{x}})$ if

$$\sigma_{\mathbf{A}, \beta_{BP}s(\cdot)} \geq \min\left\{\frac{\sigma_{min}(\mathbf{A}\mathbf{A}^T)}{\sigma_{max}(\mathbf{A}\mathbf{A}^T)}, \sigma_{\mathbf{A}, \frac{\beta_{LS}}{\sigma_{max}(\mathbf{A}\mathbf{A}^T)}s(\cdot)}\right\}. \tag{48}$$

Following the discussion below Condition B.2, note that if $\beta_{BP} \geq \beta_{LS}/\sigma_{max}(\mathbf{A}\mathbf{A}^T)$ then it is expected that $\sigma_{\mathbf{A}, \beta_{BP}s(\cdot)} \geq \sigma_{\mathbf{A}, \frac{\beta_{LS}}{\sigma_{max}(\mathbf{A}\mathbf{A}^T)}s(\cdot)}$, for which our results imply that using the BP fidelity term rather than the LS term requires less iterations *regardless* of $\frac{\sigma_{min}(\mathbf{A}\mathbf{A}^T)}{\sigma_{max}(\mathbf{A}\mathbf{A}^T)}$. Alternatively, and perhaps more useful for practitioners, the results hint that the convergence rate of BP is less affected than the convergence rate of LS by bad condition number of $\mathbf{A}\mathbf{A}^T$ (i.e., low $\frac{\sigma_{min}(\mathbf{A}\mathbf{A}^T)}{\sigma_{max}(\mathbf{A}\mathbf{A}^T)}$). In other words, we expect to see correlation between decreasing $\frac{\sigma_{min}(\mathbf{A}\mathbf{A}^T)}{\sigma_{max}(\mathbf{A}\mathbf{A}^T)}$ and increasing the difference between the convergence rate of LS and BP in favor of BP. This finding reveals an advantage in preferring BP over LS for solving ill-posed linear inverse problems that are highly ill-conditioned in the subspace spanned by the rows of \mathbf{A} .

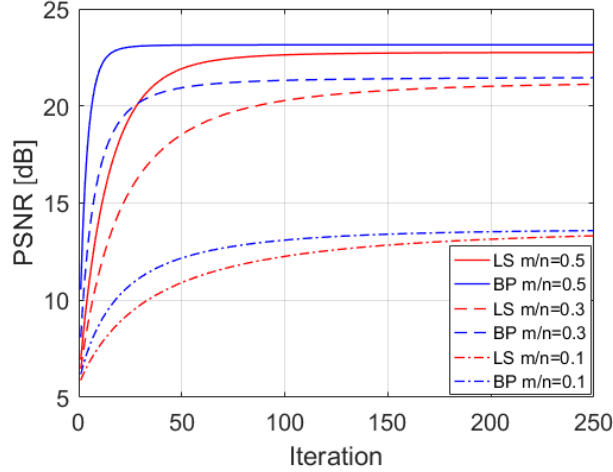


Figure 9: Compressed sensing with different m/n ratios of Gaussian measurements and SNR of 20dB. PSNR (averaged over 4 test images) of PGD with ℓ_1 prior versus iteration number (for $R = 1.5e5$). Note that in these experiments the ratio $\frac{\sigma_{\min}(\mathbf{A}\mathbf{A}^T)}{\sigma_{\max}(\mathbf{A}\mathbf{A}^T)}$ equals 0.0296, 0.0862 and 0.2721 for m/n ratios of 0.5, 0.3 and 0.1, respectively.

C. Additional Empirical Results for PGD

In this section we present more results for the experimental setting of Section 5.1. Specifically, we consider Gaussian $\mathbf{A} \in \mathbb{R}^{m \times n}$ (with i.i.d. entries drawn from $\mathcal{N}(0, 1/m)$), SNR of 20dB (with white Gaussian noise), and recovery based on PGD that uses each of LS and BP objectives with ℓ_1 -ball feasible set and Haar wavelet basis. Contrary to Section 5.1 that considers fixed $m/n = 0.5$ and modifies the regularization parameter R , here we fix $R = 1.5e5$ and modify the compression ratio m/n .

Fig. 9 shows the PSNR (averaged over the test images from Section 5.1) as a function of the iteration number, for $m/n = 0.5$, $m/n = 0.3$ and $m/n = 0.1$. Note that in these experiments the ratio $\frac{\sigma_{\min}(\mathbf{A}\mathbf{A}^T)}{\sigma_{\max}(\mathbf{A}\mathbf{A}^T)}$ equals 0.0296, 0.0862 and 0.2721 for m/n ratios of 0.5, 0.3 and 0.1, respectively. Observing the convergence rates of the different curves in this figure, it is easy to see that the advantage of the rate of BP over the rate of LS increases when the ratio m/n increases, or alternatively when the ratio $\frac{\sigma_{\min}(\mathbf{A}\mathbf{A}^T)}{\sigma_{\max}(\mathbf{A}\mathbf{A}^T)}$ decreases.

The empirical behavior above is inline with the results of the analysis in both Section 3.3 and Appendix B. Regarding Section 3.3, which characterizes the ratio between the convergence rates of LS and BP using the ratio of the terms P_{LS} and P_{BP} , we see agreement with the curves in Fig. 1a, where the approximate ratio of P_{BP}/P_{LS} decreases (i.e., bigger advantage for BP) when the ratio m/n increases. Regarding Appendix B⁸ the results in (46) and (47) suggest that the convergence rate of BP is less affected than the convergence rate of LS by bad condition number of $\mathbf{A}\mathbf{A}^T$, i.e., low values of $\frac{\sigma_{\min}(\mathbf{A}\mathbf{A}^T)}{\sigma_{\max}(\mathbf{A}\mathbf{A}^T)}$. Again, this agrees with the results in Fig. 9.

⁸Note that Appendix B considers the more general proximal gradient method. However, PGD with convex feasible set is subsumed in this setting, since it is essentially proximal gradient method for $s(\cdot)$ which is a convex indicator.